Numerical Study on Optics and Heat Transfer of Solar Reactor for Methane Thermal Decomposition

Haneol Kim [1,2] and Jongkyu Kim [1,*]

1 Renewable Heat Integration Laboratory, New and Renewable Energy Institute, Korea Institute of Energy Research, Daejeon 34129, Korea; kimskyq@kier.re.kr
2 Department of Mechanical Engineering, Inha University, Incheon 22212, Korea
* Correspondence: rnokim@kier.re.kr; Tel.: +82-42-860-3477

Abstract: This study aims to reduce greenhouse gas emissions to the atmosphere and effectively utilize wasted resources by converting methane, the main component of biogas, into hydrogen. Therefore, a reactor was developed to decompose methane into carbon and hydrogen using solar thermal sources instead of traditional energy sources, such as coal and petroleum. The optical distributions were analyzed using TracePro, a Monte Carlo ray-tracing-based program. In addition, Fluent, a computational fluid dynamics program, was used for the heat and mass transfer, and chemical reaction. The cylindrical indirect heating reactor rotates at a constant speed to prevent damage by the heat source concentrated at the solar furnace. The inside of the reactor was filled with a porous catalyst for methane decomposition, and the outside was surrounded by insulation to reduce heat loss. The performance of the reactor, according to the cavity model, was calculated when solar heat was concentrated on the reactor surface and methane was supplied into the reactor in an environment with a solar irradiance of 700 W/m^2, wind speed of 1 m/s, and outdoor temperature of 25 °C. As a result, temperature, methane mass fraction distribution, and heat loss amounts for the two cavities were obtained, and it was found that the effect on the conversion rate was largely dependent on a temperature over 1000 °C in the reactor. Moreover, the heat loss of the full-cavity model decreased by 12.5% and the methane conversion rate increased by 33.5%, compared to the semi-cavity model. In conclusion, the high-temperature environment of the reactor has a significant effect on the increase in conversion rate, with an additional effect of reducing heat loss.

Keywords: methane; decomposition; reactor; cavity; solar thermal; numerical simulation; optical; heat transfer; chemical reaction

1. Introduction

As the problems of global warming, caused by the use of fossil fuels, have increased, it has become necessary to expand the use of renewable energy to reduce greenhouse gas emissions. Among these renewable energies, hydrogen is attracting attention as an eco-friendly energy source that does not generate pollutants during combustion. In particular, to take a leadership role in terms of a hydrogen economy, South Korea is attempting to build a strong hydrogen vehicle and fuel cell-based industrial ecosystem, and to create a hydrogen production and supply system without carbon emissions. Hydrogen is generally produced through methane reforming, water electrolysis, and thermal decomposition, among various other processes. When fossil fuels are used to supply heat or electricity, carbon dioxide is emitted. The thermal decomposition of methane requires high-temperature heat, as shown in Equation (1). If concentrated solar energy is used, energy that is capable of producing hydrogen from methane can be provided without carbon emissions. The temperature required for obtaining a reasonable yield from methane,

through thermal decomposition, is above 1200 °C. If a catalyst is used, the temperature required for decomposition can be considerably reduced [1–3].

$$CH_4 \rightarrow C + 2H_2 \quad \Delta H_{298}^o = 75.6 \text{ kJ/mol} \tag{1}$$
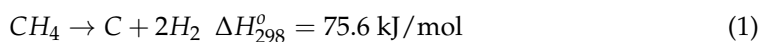
Research on methane thermal decomposition using solar thermal technology has been conducted since the early 2000s. Abanades et al. developed a methane decomposition reactor, the body of which was stainless steel, and the graphite tube mounted inside was directly heated by concentrated solar heat through a window. They developed a performance prediction model and compared it with the experimental results for verification [4,5]. Magg et al. developed and experimented with a 5 kW directly heated methane decomposition reactor equipped with a circular quartz window of a cylindrical cavity [6]. Also, Hirsch et al. conducted experiments by adding helical caving to the inner wall of the same reactor to improve the performance [7]. In addition, Ozalp et al. conducted a simulation of the heat transfer and methane decomposition, according to the presence or absence of helical caving inside this reactor, to compare the performance [8]. Yeheskel et al. developed a directly heated volumetric reactor, optimized through computational fluid dynamics (CFD). Experiments were also conducted to produce hydrogen and carbon materials from methane using a reactor characterized by a high reaction temperature, transparent window protection, and directional streaming flow (tornado) [9].

Most indirect reactors are of a tubular type. Rodat et al. used a 10 kW reactor, in which methane was injected inside the tube in a high-temperature environment when the graphite tube reactor located in the graphite cavity was heated, after the concentrated solar heat passed through the opening. The heat transfer and reaction were calculated through a heat flow analysis and compared with the experimental results [10,11]. Subsequently, the experiment was conducted by scaling up with a 50 kW methane decomposition reactor for a solar furnace, and a conversion rate of 72–100% was achieved at a higher flow rate than before [12]. Valdes-Parada et al. developed a reactor equipped with a vertical graphite reaction tube inside a cubic cavity, with a quartz window that absorbs concentrated solar heat. The tube is composed of two concentric tubes to improve the flow path in the reaction tube and secure the residence time. At this time, the temperature distribution and methane conversion rate were numerically simulated by supplying an argon–methane mixture, and the relationship between the temperature distribution and the conversion rate was determined by comparing it with the experimental results. Based on this, it was intended to be utilized in the development of a reactor for light hydrocarbons [13].

The direct heating reactor is advantageous for heating the reactants, in terms of heat transfer, because solar heat is directly concentrated inside, as shown in Figure 1. However, since the reach distance of concentrated sunlight is limited, and it is not long due to space constraints, there is a large temperature difference between the area where light reaches and the area where it does not. Also, carbon particles produced during the reaction are deposited at a mounted quartz window that transmits light internally, resulting in damage due to reduced transmittance and increased temperature. In addition, there is a limit to the reactor volume, due to the limitation of the window fabrication size.
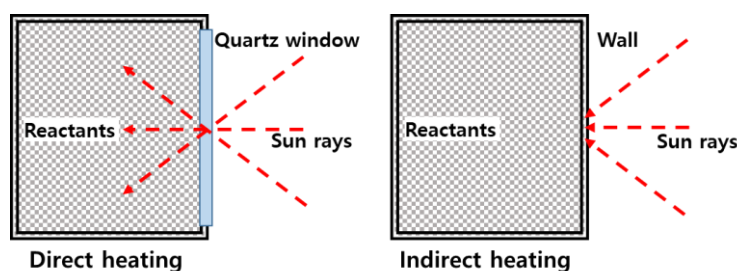

Figure 1. Direct and indirect heating reactor.

The indirect heating reactor has a cavity for insulation outside the reactor, as in the aforementioned study. Inside the cavity, the reactor, mainly in the form of a bundle of graphite tubes, is installed to allow the methane or methane mixture to react.

A high temperature of 1200 °C or higher is required to decompose methane. If the catalyst is applied, the reaction temperature can be lowered by reducing the activation energy required for methane decomposition, and the heat loss and damage generated in the reactor can be reduced. Although differences depend on the applied test environment, in general, methane can be decomposed in the range of 900~1100 °C, by using a catalyst. Representatively, in the case of the BP2000 catalyst, a methane–hydrogen conversion of 9.1% was achieved at 850 °C. Carbon black (CB) or activated carbon (AC) catalysts are mainly used as thermal decomposition catalysts. The research on methane decomposition catalysts has been steadily progressing [14–18]. Suelves et al. monitored the mass change over time during the thermal catalytic decomposition of methane, for CB and AC catalysts, and proved that among the catalysts, BP2000, a CB series, deposited the largest amount of carbon before deactivation [16].

In this study, optical distribution, heat and mass transfer, and chemical reaction simulations were performed to develop an indirectly heated methane decomposition reactor, using solar thermal as a heat source. The actual experimentation of the reactors used in solar furnaces has difficulties, such as cloudy weather conditions and high-temperature environments over 1000 °C. Therefore, predicting results through simulations is time and cost effective. A rotary cylindrical reactor was designed to secure the reactor processing flow and receive heat uniformly from the solar furnace. In addition, to reduce the heat loss of the existing semi-cavity, and increase the methane–hydrogen conversion, a full cavity with improved insulation performance was designed and the reactor performance, according to each cavity model, was compared.

The paper is structured as follows: Section 2 contains the methane decomposition reactor system, which has a parabolic reflector, reactor, and catalyst. Section 3 explains the simulation methods for optical, thermal, and chemical reactions. Section 4 brings the simulation results for heat loss and methane conversion. Section 5 outlines the conclusions obtained from the study.

2. Methane Thermal Decomposition Reactor System

2.1. Parabolic Reflector

Regarding the parabolic reflector used in the analysis, the specifications of a 40 kW$_{th}$ solar furnace, installed at the Korea Institute of Energy Research, were applied, as shown in Figure 2 [19].


Figure 2. 40 kW$_{th}$ solar furnace at KIER.

The solar furnace is composed of a heliostat, parabolic reflector, and blind. Solar energy is transferred to the parabolic reflector through a heliostat, which tracks the sun and is eventually concentrated on the reactor surface located at the focal point, resulting in high-temperature heat.

The blind is located between the heliostat and parabolic reflector to control the amount of sunlight by controlling the opening and closing rate. However, in this calculation, only a parabolic reflector was applied to the simulation, assuming that the sunlight reflected from the heliostat illuminates all sides of the parabolic reflector and completely opens the blind. Instead, the optical efficiency was calculated by considering the reflectance of the heliostat and the loss of the reflective area, owing to the thickness of the blind.

Therefore, the reflectance of the heliostat and the parabolic reflector, measured by a spectrometer, is 84% and 94%, respectively, and the effective area ratio is 85%, owing to blocking that occurs from the pure structural thickness of the parabolic reflector and blind. In the calculation, an overall optical efficiency of 67% is applied to the parabolic reflector. The mirrors applied to the heliostat and parabolic reflector are coated with aluminum in the same way, but the thicknesses are 3.2 mm and 1mm, respectively, which causes a difference in reflectivity.

As shown in Figure 3, the parabolic reflector has an external diameter of 9.0 m and an internal diameter of 1.5 m, with a pure mirror area of 55.38 m^2 and a focal distance of 4.98 m. When the reactor is located at the focal point of the concentrator, the thermal fatigue is high, owing to the narrow heating area with a high peak flux, which reduces the durability of the reactor. To improve this, the reactor was placed 100 mm behind the focal position to reduce the peak flux and expand the heating area.
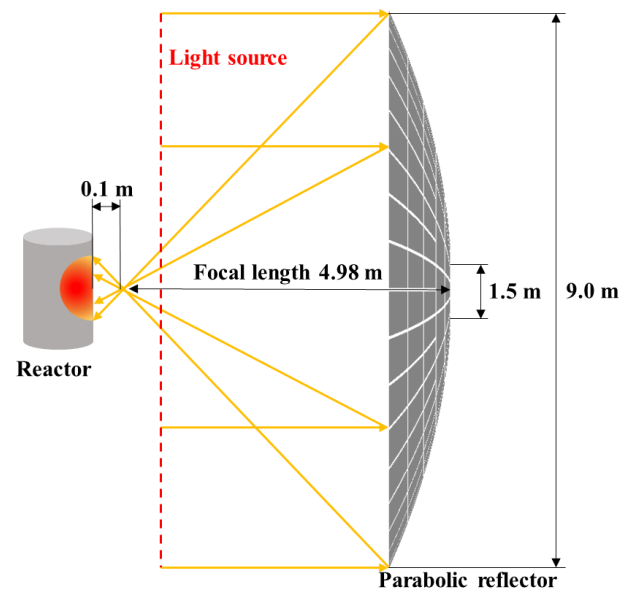
Figure 3. Parabolic reflector.

2.2. Reactor

The reactor is made of 310S stainless steel (STS 310S), and has a cylindrical shape with an internal diameter of 208.3 mm, a height of 315 mm, and a thickness of 4 mm, and the inside is filled with catalysts. The reactor is rotated to prevent rapid heat damage caused by continuous exposure to the fixed focused light to the reactor, and to supply a uniform heat flux at the circumference of the reactor. For this purpose, a motor, reducer, and rotary joint are installed at the top and bottom of the reactor, and the rotation speed is 2.54 rad/s.

According to the thermal analysis, a thermal amount of 7.5 kW$_{th}$ is required for 80% decomposition after reaching 1000 °C, by supplying a temperature of 25 °C and 5 Nm^3/h of methane to the reactor. Among them, 3.8 kW is used for heating and 3.7 kW is used for chemical reactions. In addition, the radiation heat loss of 11.7 kW at a reactor surface

temperature of 1400 °C, with a view factor of 0.14 and aperture size of 275 × 235 mm, is considered. When a direct normal irradiance of 700 W/m^2 is supplied to the solar furnace, about 24.7 kW of heat can be obtained. Therefore, it was judged that the amount of heat supplied was sufficient, and a semi-cavity with a simple structure was designed, as shown in Figure 4. The thickness of the cavity insulation material is 50 mm or more, and it surrounds the reactor, and the front side, to which light is concentrated, is open, so that the reactor and the external environment are in direct contact. The front of the cavity is equipped with an insulation board with an aperture to allow for concentrated light to enter and prevent thermal damage to the surrounding equipment and reactor flanges.
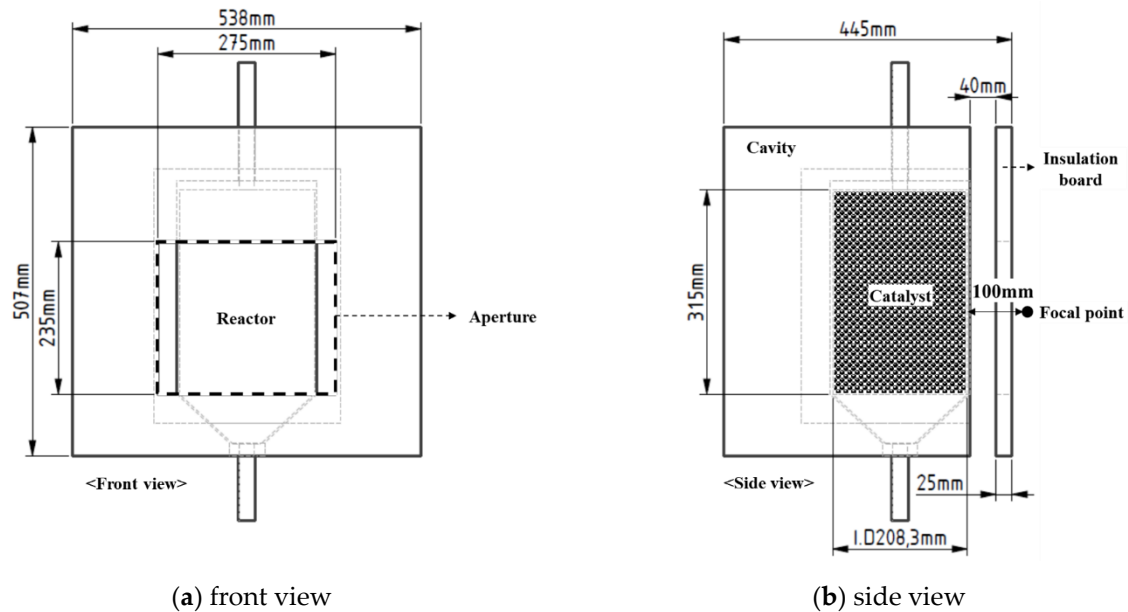

(**a**) front view　　　　　　　　　　　　　　　　　　　　(**b**) side view

Figure 4. Semi-cavity reactor model.

As shown in Figure 5, the reactor and semi-cavity were mounted on the solar furnace and preliminary tests were carried out. Through this, it was confirmed that more significant heat loss occurred than was expected. To reduce convection and radiation heat losses from the reactor, by improving the cavity performance, the space between the cavity and the front insulation board was filled with a thermal insulation board/blanket and modeled as a full cavity, as shown in Figure 6. Therefore, as the space inside the cavity is reduced, the view factor between the reactor and the outside is reduced. Using TracePro, an optical calculation program, it was confirmed that 99% of the sunlight was concentrated within 150 mm in diameter, at the focal point of the solar furnace, and the aperture size was modified. Accordingly, the aperture area of the full cavity was reduced by 38%, from 275 × 235 mm in the semi-cavity to 200 × 200 mm in the full cavity. The optical calculation method is described in detail in Section 3. For the optical and CFD calculations, 3D modeling was conducted for each cavity, as shown in Figure 7.

2.3. Catalyst

When methane is thermally decomposed, carbon black and hydrogen can be obtained. This typically requires a high temperature of 1200 °C or higher, although the use of a catalyst can reduce the activation energy for methane decomposition, which reduces the reaction temperature. Figure 8 shows the difference in activation energy when BP-2000 was used as a catalyst [14,17].

Figure 5. Installed reactor in a solar furnace.

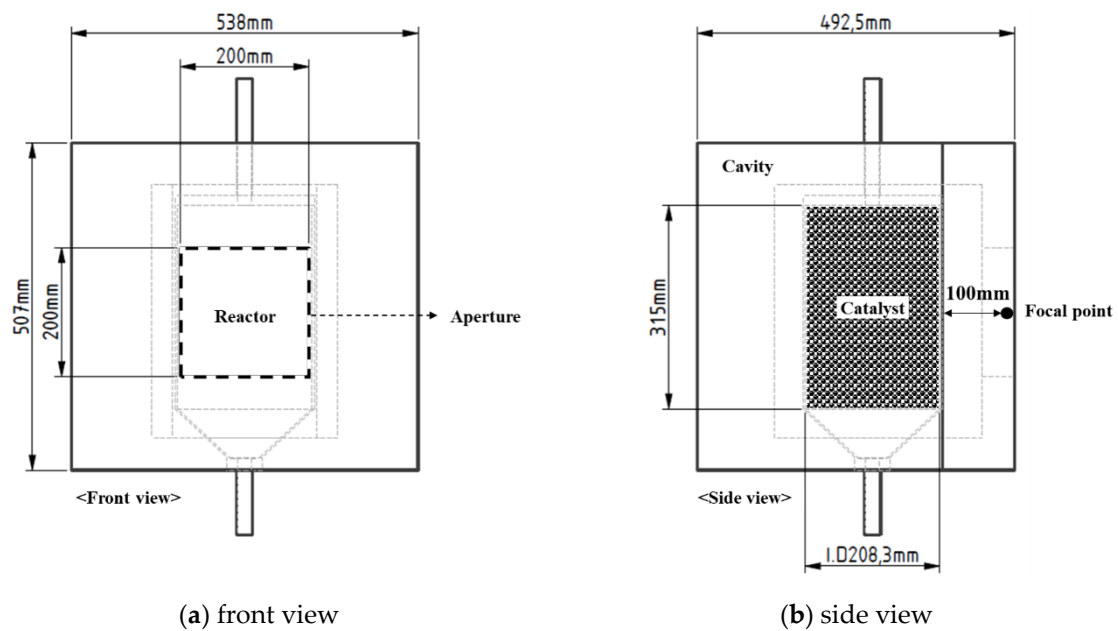(**a**) front view　　　　　　　　　　　　　　　　　(**b**) side view

Figure 6. Full-cavity reactor model.

Carbon black (CB) or activated carbon (AC) catalysts are mainly used for the thermal decomposition of methane; AC catalysts have a relatively high initial reaction rate and a small amount of carbon black is produced before deactivation. Conversely, CB catalysts have a low initial reaction rate, but long and constant catalytic activity, resulting in large amounts of carbon black before deactivation. CB catalysts are suitable for the maximum prevention of catalyst deactivation during daylight hours, and to ensure the production of hydrogen and carbon black in practical experiments [14–18]. Therefore, in this study, among CB catalysts, BP-2000, which shows a high hydrogen production rate before deactivation, and is a commercial product, was adopted, and the characteristics are shown in Table 1 [14].
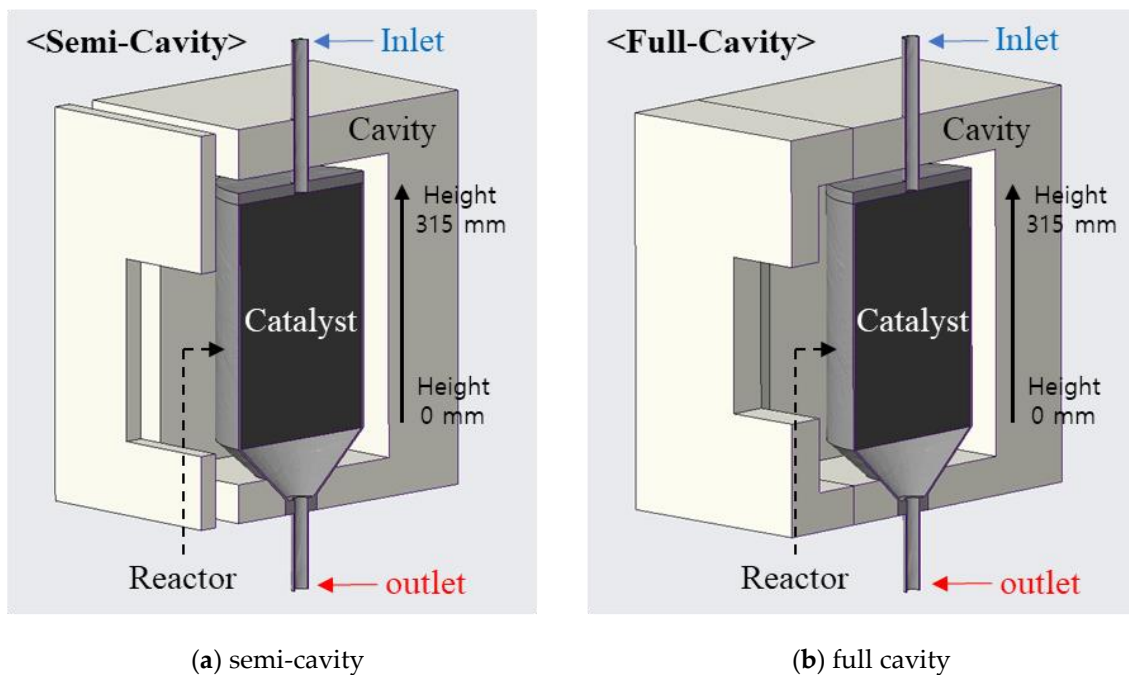
(**a**) semi-cavity   (**b**) full cavity

Figure 7. 3D modeling of reactor and cavity.
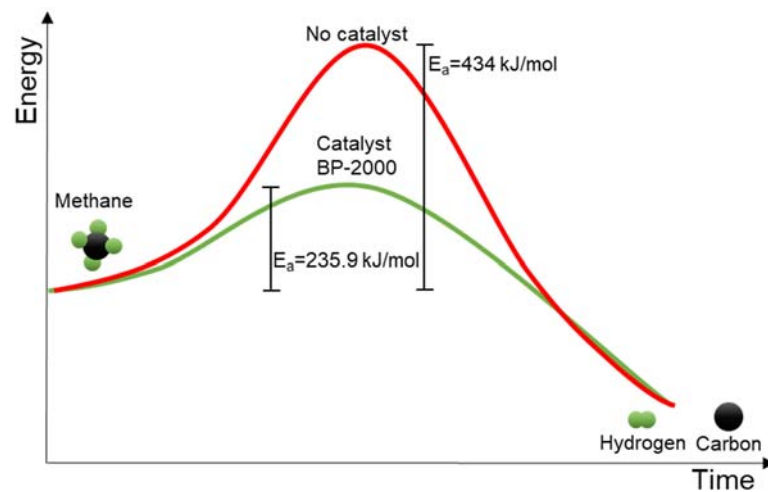
Figure 8. Difference in activation energy w/wo catalyst.

Table 1. Properties of BP-2000 [14].

Item	Value
surface area (m^2/g)	1500
pre-exponential factor, k_0 (s^{-1})	4.3×10^9
activation energy, E_a (kJ/mol)	235.9

3. Simulation Method

3.1. Optical Method

To calculate the amount of heat concentrated at the reactor through the parabolic reflector, an optical software, TracePro, based on the Monte Carlo ray-tracing method, is used. The circular light source is located 4 m away from the parabolic reflector, and the diameter is set to 9 m to cover the entire area of the parabolic reflector. Considering the solar radiation conditions in the area where the reactor is installed, the direct normal irradiance is set to an average of 700 W/m^2.

The actual solar beam radiation does not radiate uniformly from the sun, but decreases in intensity as it moves from the center to the radius. This is called limb darkening and the light intensity is a function of the sun's radius angle. Limb darkening should be considered to calculate realistic concentrating shape, and Figure 9 shows the Allen, Buie and Pillbox models presented in the literature. The Pillbox model is suitable for simple calculations, but differs from the actual solar beam, and the TracePro software used in this study can calculate the intensity of light for each radius based on the Allen model [20]. Even compared with the recently presented Buie's model, the error is about 3% in the region where the angular displacement is 0 to 4.65 mrad, which is not much different [21].
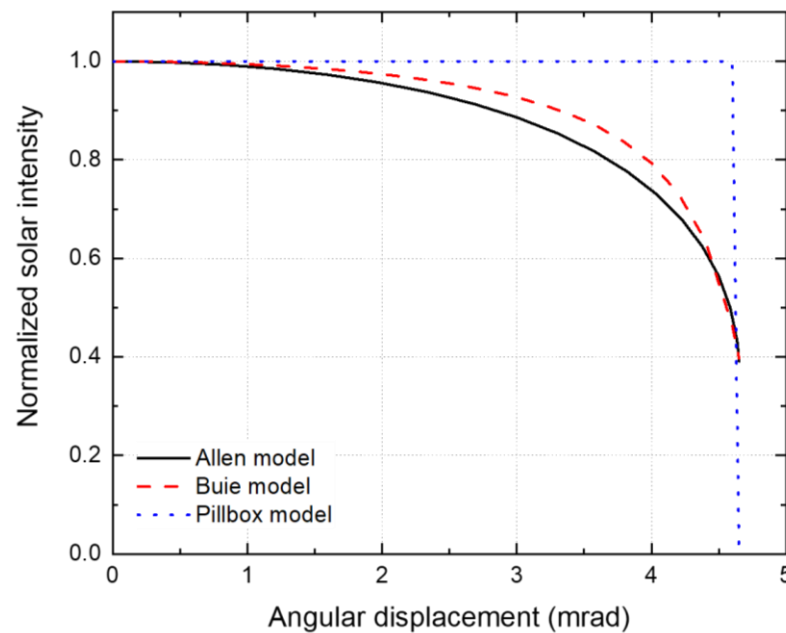

Figure 9. Solar limb-darkening models.

The reflectance of the parabolic reflector is based on a total optical efficiency of 67%, as previously mentioned. In TracePro, an absorption rate of the reactor and the ceramic insulation can be set to calculate the optical loss. However, since the thermal and chemical reactions calculated via CFD also contain a radiation model, the absorption rate in optical calculations is set to zero to avoid duplication. The amount of heat collected in the reactor system can be calculated as shown in Equation (2).

$$Concentrated\ heat = Irradiance \times Dish\ area \times Total\ optical\ efficiency \qquad (2)$$

Optical Distributions

To calculate heat transfer and chemical reaction through CFD, optical distributions are calculated first and used as input conditions. Reactor 3D models according to the parabolic reflector and cavity shape are applied, and about 2 million rays are irradiated to the reflector to calculate the heat flux concentrated at the reactor and cavity. Firstly, the distributions of heat flux on the reactor surface according to the focal distance from the reflector are calculated as shown in Figure 10, and the total amount of heat received and the peak heat flux on the reactor are listed in Table 2. Additionally, the heat flux profiles at the reactor surface according to the focal distance are shown in Figure 11. Under the condition of 700 W/m^2 of solar irradiance, the total amount of heat reflected from the parabolic reflector is 24.71 kW. If the reactor is located 70 mm in front the focal point, a total of 20.4 kW of the thermal amount is concentrated. However, as shown in Table 2, most of the thermal energy is concentrated at the center, resulting in an extremely high peak flux of 1720.6 kW/m^2. This makes it difficult to heat the reactor uniformly and can cause damage to the surface of the reactor within a short time, owing to a high flux. If the

reactor is located 130 mm from the focal point, the peak flux is lowered to 527.3 kW/m^2 at the center, which is advantageous in terms of its durability, but is inefficient because only approximately 58% of the heat provided by the parabolic reflector is concentrated at the reactor. If the reactor is located 100 mm behind the focal point, it is at the middle position of the previous two cases, and approximately 70% of the heat reflected from the parabolic reflector is concentrated at the reactor.
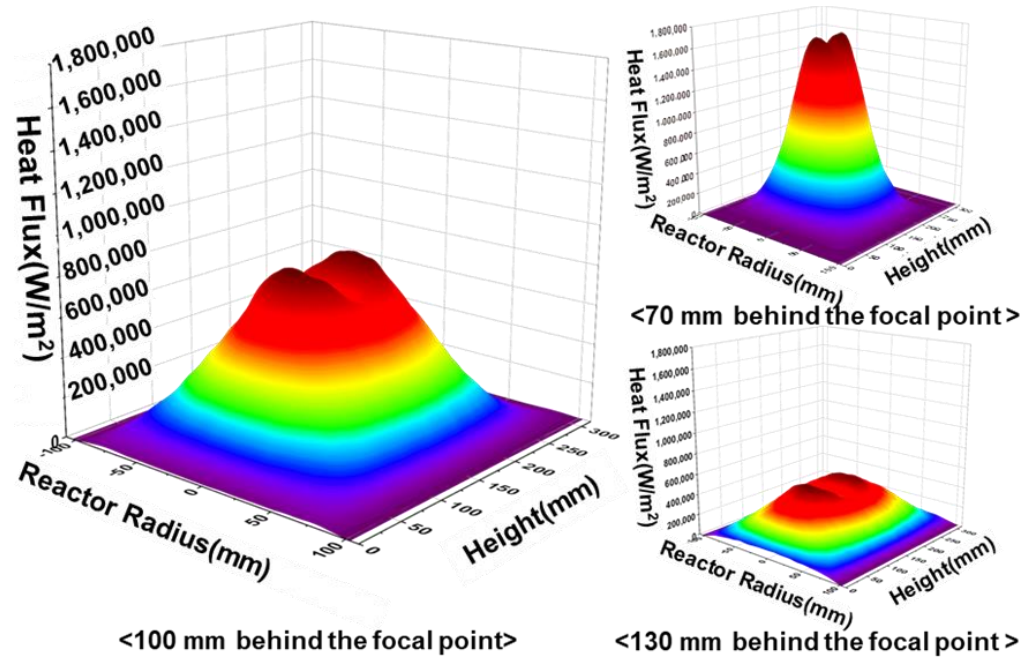

Figure 10. Heat flux distributions depending on the focal distance.

Table 2. Thermal amounts at the reactor surface according to the focal distance.

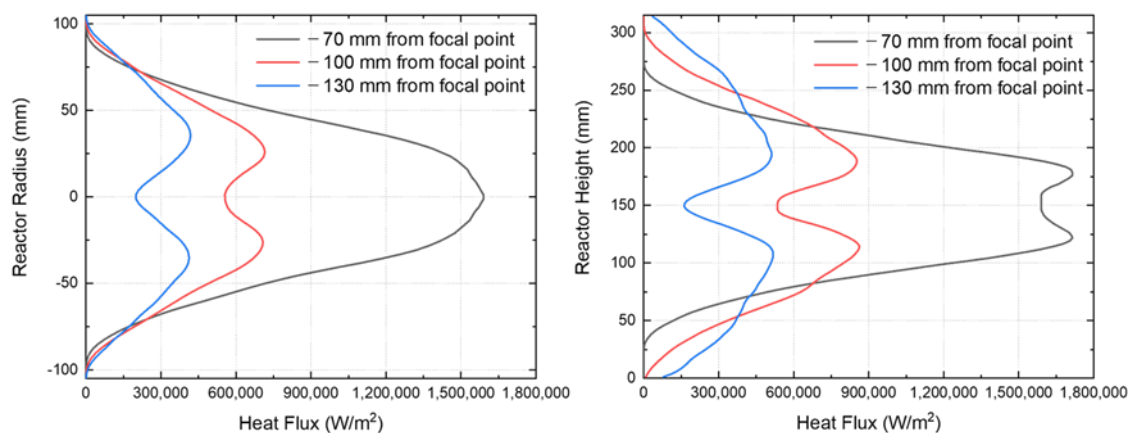| Distance from Focal Point (mm)	Total Power (kW)	Peak Flux (kW/m^2)
70	20.4	1720.6
100	17.2	865.5
130	14.4	527.3

Figure 11. Heat flux distributions at the reactor surface depending on the focal distance according to reactor radius (**left**) and reactor height (**right**).

Therefore, to improve the durability of the reactor and for effective heat transfer, the reactor is positioned 100 mm behind the focal point and optical calculations are performed for the semi-cavity model and the full-cavity model. Figure 12 shows the solar ray in the optical calculation of a semi-cavity that is 100 mm after the focal point.
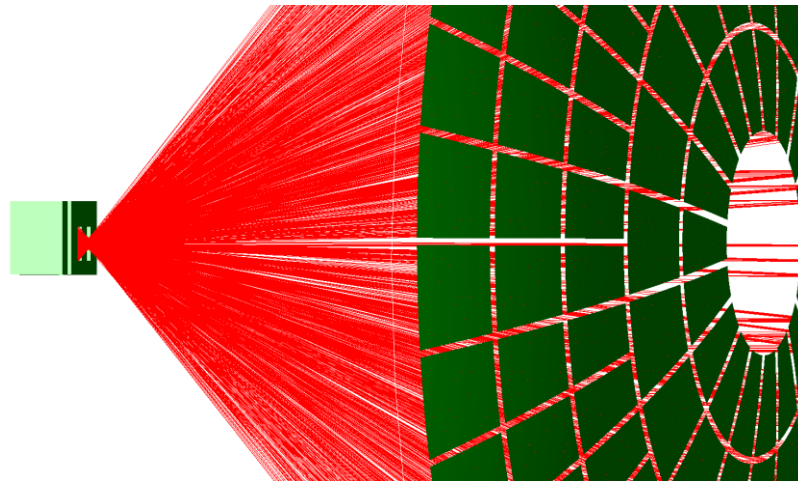

Figure 12. Optical calculation with TracePro.

In both cavity models, the solar ray distribution concentrated on the inner wall of the cavity and reactor surface is shown in Figure 13. For both models, the size of the aperture is greater than the focal area, and thus there is no loss due to blocking at the front insulation board. According to the analysis, approximately 70% of the total ray is distributed at the reactor surface, and the remaining 30% is distributed at the left and right inner walls of the cavity.
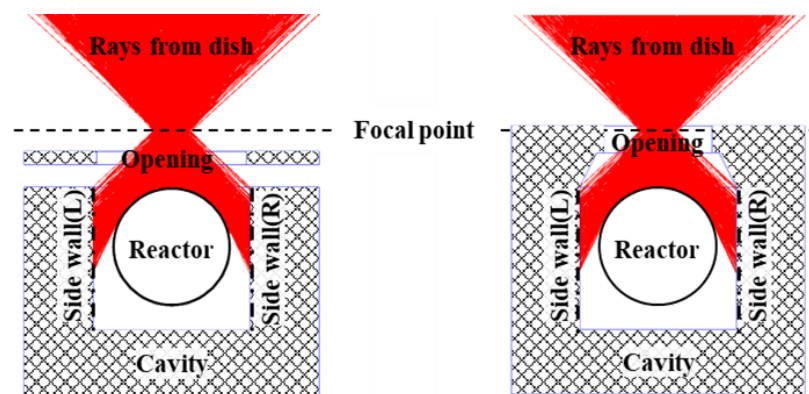

Figure 13. Sun ray distributions in semi-cavity (**left**) and full cavity (**right**).

The distribution of the concentrated heat flux at the left and right inner walls of the two cavities is approximately the same, as shown in Table 3 and Figure 14. This is because the reactor shapes, focal distance, and inner walls of the cavity side are identical despite the difference in the cavity shapes of the two models. Based on the semi-cavity model, out of the total thermal amount of 24.71 kW, the reactors absorb 16.88 kW, and the inner walls of the left and right cavity absorb 3.60 kW, respectively.

In order to import the optical calculation results as the heat source boundary conditions for the CFD calculation, the two-dimensional heat flux distribution data of the reactor and cavity surface are converted into profile data of three-dimensional x, y, z coordinates. For this purpose, the same coordinate system is used for optical and CFD calculations, and the boundary of the reactor and cavity is assumed to be a virtual cell with very thin thickness

to read the heat generation rate value as a radiation source term in Equation (7) in the CFD as shown in Figure 15.

Table 3. Concentrated heat amounts according to location in the cavity.

	Semi-Cavity		Full Cavity	
Item	**Thermal Amount (kW)**	**Ratio (%)**	**Thermal Amount (kW)**	**Ratio (%)**
reactor	16.88	68.3	17.23	69.7
inner wall (left)	3.60	14.6	3.65	14.8
inner wall (right)	3.60	14.6	3.65	14.8
etc.	0.63	2.5	0.18	0.7
total	24.71	100	24.71	100
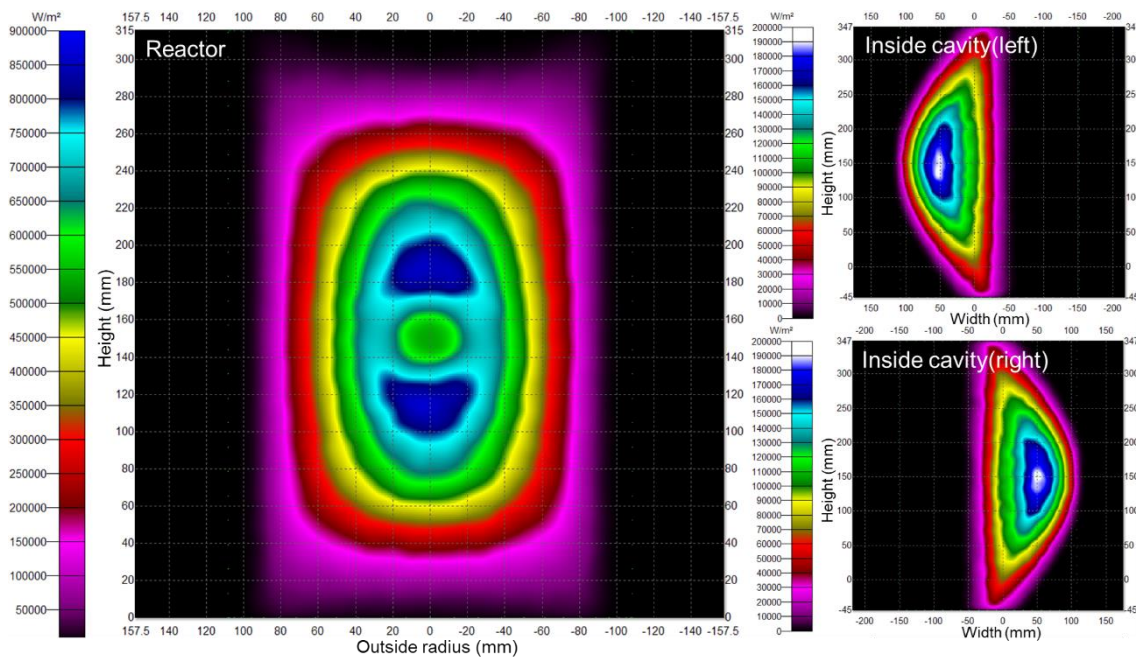
Figure 14. Heat flux (W/m^2) distributions obtained from optic calculation (full cavity).
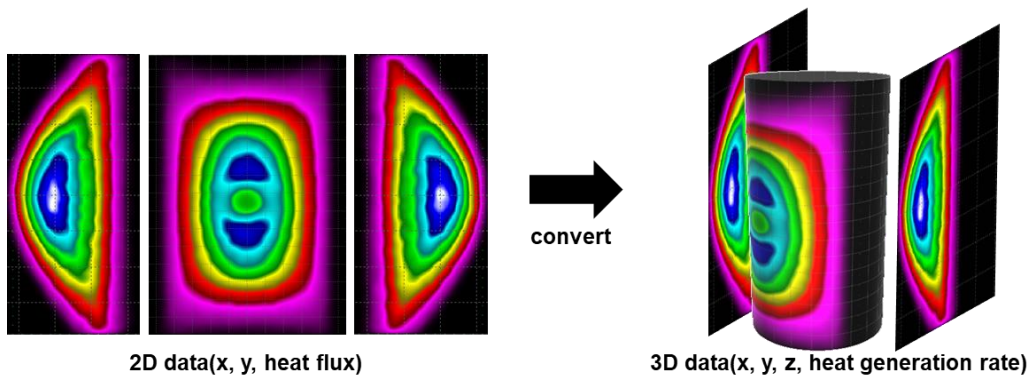

Figure 15. Transformation of 2D optical results to 3D CFD boundary condition.

3.2. Thermal and Chemical Calculation Method

The commercial program Ansys Fluent 19.0 is used to simulate the methane decomposition reaction of the reactor system. The calculation domains are constructed for the reactor

systems and the surrounding environment, as shown in Figure 16; the size of which is set to 6 m × 6 m × 6 m, more than 10 times the size of the cavity. Approximately 7,000,000 tetrahedral meshes are used for the calculations. The skewness of the calculation mesh has a mean value of 0.25, a maximum value of 0.85, an average value of 0.85, and a minimum value of 0.20.

(**a**) calculation domain   (**b**) reactor and cavity
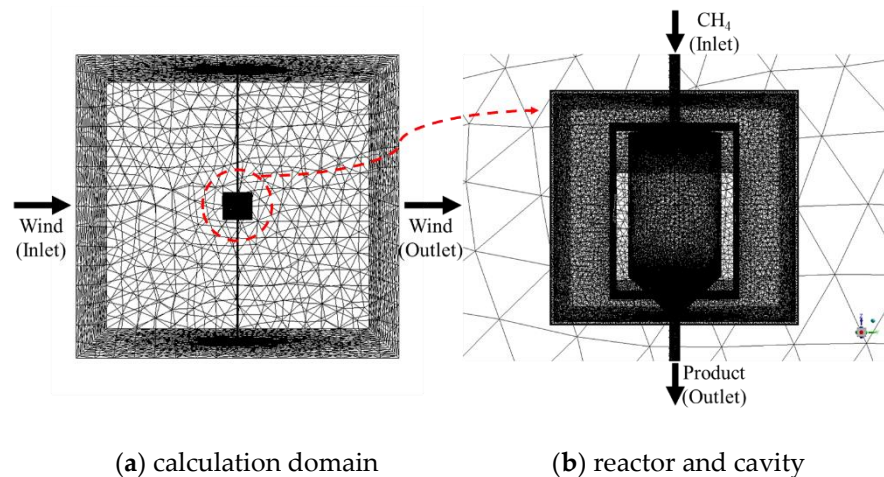
Figure 16. Reactor and cavity calculation domain for CFD simulation (semi-cavity model).

In addition, to calculate the heat loss from the reactor and cavity, the ambient temperature, wind direction and wind speed are set in consideration of the installation location. Because the cavity is located inside the solar furnace, the wind speed is assumed to be at a low speed of approximately 1 m/s, and the wind direction is set in a lateral direction where the heat loss could be relatively high. This time, the ambient temperature is 25 °C.

The reactor is constantly rotated through Fluent's frame motion function along its central axis at the same speed of 2.54 rad/s as the real system. In addition, the BP-2000 catalyst with a porosity of 0.76 is filled inside the reactor. At 25 °C, 5 Nm^3/h of methane is fed through the reactor inlet for methane decomposition. The standard k-epsilon model is used for the calculation of turbulent flow fields within and outside the reactor. The continuum, momentum, k-epsilon, and energy equations used in the calculations are as shown in Equations (3)–(7).

The continuity equation is as follows:

$$\frac{\partial \rho}{\partial t} + \nabla \cdot \left(\rho \vec{v} \right) = 0. \tag{3}$$

The momentum equation is as follows:

$$\frac{\partial}{\partial t} \left(\rho \vec{v} \right) + \nabla \cdot \left(\rho \vec{v} \vec{v} \right) = -\nabla p + \nabla \cdot \left(\overline{\overline{\tau}} \right) + \rho \vec{g} + \vec{F}. \tag{4}$$

The k-equation is as follows:

$$\frac{\partial}{\partial t}(\rho k) + \frac{\partial}{\partial x_i}(\rho k u_i) = \frac{\partial}{\partial x_j}\left[\left(\mu + \frac{\mu_t}{\sigma_k} \right) \frac{\partial k}{\partial x_j} \right] + G_k + G_b - \rho \varepsilon. \tag{5}$$

The ε-equation is as follows:

$$\frac{\partial}{\partial t}(\rho \varepsilon) + \frac{\partial}{\partial x_i}(\rho \varepsilon u_i) = \frac{\partial}{\partial x_j}\left[\left(\mu + \frac{\mu_t}{\sigma_\varepsilon} \right) \frac{\partial \varepsilon}{\partial x_j} \right] + C_{1\varepsilon}\frac{\varepsilon}{k}(G_k + C_{3\varepsilon}G_b) - C_{2\varepsilon}\rho\frac{\varepsilon^2}{k}. \tag{6}$$

The energy equation is as follows:

$$\frac{\partial}{\partial t}(\rho E) + \nabla\cdot\left(\vec{v}\left(\rho E + p\right)\right) = \nabla\cdot\left(k_{eff}\nabla T - \sum_j h_j\vec{J_j} + \left(\bar{\bar{\tau}}_{eff}\cdot\vec{v}\right)\right) + S_{reaction} + S_{radiation},\tag{7}$$

where $\mu_t = \rho C_\mu \frac{k^2}{\varepsilon}$,
$C_{1\varepsilon} = 1.44$, $C_{2\varepsilon} = 1.92$, $C_\mu = 0.09$, $\sigma_k = 1.0$, $\sigma_\varepsilon = 1.3$,
$C_{3\varepsilon} = tanh\left|\frac{v}{u}\right|$,
$k_{eff} = k + k_t$,
$E = h - \frac{p}{\rho} + \frac{v^2}{2}$,
$h = \sum_j Y_j h_j$,
$h_j = \int_{T_{ref}}^T c_{p,j} dT$.

3.2.1. Radiation Model—S2S

A surface-to-surface (S2S) model is applied to calculate the radiation heat transfer according to the size, distance, and direction of each surface within the calculation domain. Through this model, the radiation loss and view factor from each surface of the cavity and reactor to each surrounding wall can be obtained. Each surface is uniformly radiated in all directions, regardless of the incoming direction, with the same radiation and absorption rates under the assumption of a gray and diffuse surface. The energy emitted from a given surface through the S2S model is calculated using Equation (8).

$$q_{out,i} = \varepsilon_i \sigma T_i^4 + \rho_i \sum_{j=1}^N F_{ij}q_{out,j}\tag{8}$$

where the view factor F_{ij}, which is a geometric function between the two surfaces i and j, is calculated using Equation (9).

$$F_{ij} = \frac{1}{A_i}\int_{A_i}\int_{A_j}\frac{cos\theta_i cos\theta_j}{\pi r^2}\delta_{ij}dA_i dA_j\tag{9}$$

3.2.2. Species Transport and Finite Rate

The species transport and finite-rate model are applied to calculate the methane decomposition reaction by the catalyst in the reactor. Therefore, the conservation equation for a chemical species is given by Equation (10). To calculate the term R_i, which is the net rate of production by a chemical reaction, the rate constant k_r is required. For this, a 1-step Arrhenius-type reaction equation is applied, as shown in Equation (11). For the pre-exponential factor k_0 and activation energy E_a, as shown in Table 1, the BP-2000 material property values of 4.3×109 s^{-1} and 235.9 kJ/mol are used, respectively.

For the species transport, the following equation is used:

$$\frac{\partial}{\partial t}(\rho Y_i) + \nabla\cdot\left(\rho\vec{v}Y_i\right) = -\nabla\cdot\vec{J}_i + R_i.\tag{10}$$

For the finite rate, the following equation is used:

$$k_r = k_0 \exp\left(\frac{-E_a}{RT}\right).\tag{11}$$

4. Results and Discussion

4.1. Thermal Loss of Reactor

In the calculation, 1300 and 1105 iterations of the semi-cavity model and full-cavity model are performed for convergence, respectively. Differences occur because the mesh configuration is different according to the cavity shape in the calculation. However, in both

models, the convergence conditions of 10^{-3} for continuity, velocity and k-epsilon, and 10^{-6} for energy and species transport are the same, so the results are not affected.

The radiation and convective heat losses in each reactor model are listed in Table 4. In the case of the semi-cavity, 9.33 and 8.15 kW are generated, owing to radiation and convective heat losses, respectively, and 9.44 and 5.85 kW are generated in the case of the full cavity. To analyze this, the temperature contour and outside reactor air velocity vector distributions of the two reactor model cross-sections are compared, as shown in Figure 17.

Table 4. Heat loss according to cavity shape.

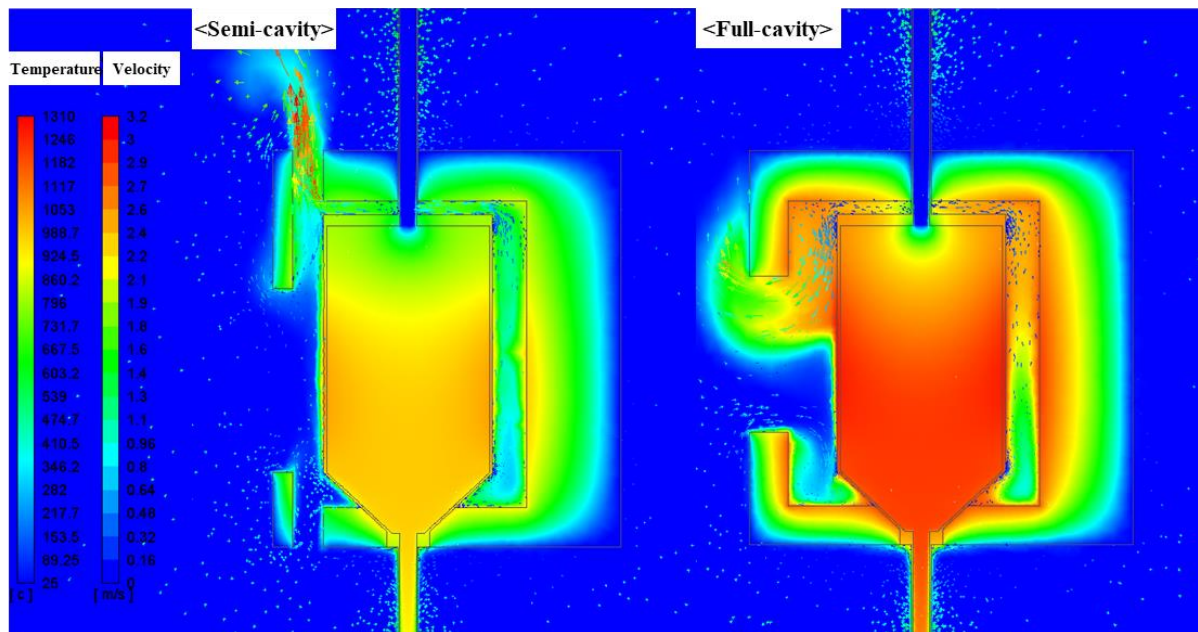|	Semi-Cavity		Full Cavity	
Item	**Thermal Amount (kW)**	**Ratio (%)**	**Thermal Amount (kW)**	**Ratio (%)**
radiation heat loss	9.33	53.4	9.44	61.7
convection heat loss	8.15	46.6	5.85	38.3
total	17.48	100	15.29	100

Figure 17. Temperature contour and air velocity vector distributions of center vertical cross-section of semi-cavity (**left**) and full cavity (**right**).

In the case of the semi-cavity model, the high-temperature air around the reactor travels out to the open space above the cavity, and the low-temperature outside air flows in to fill it, and thus the temperature of the reactor wall decreases. On the contrary, in the full-cavity model, the entire reactor, except the opening aperture, is surrounded by a cavity, and thus the air heated inside does not leak to the outside immediately, and stays in the upper space. As a result, a higher-temperature environment is provided for the reactor and the space inside the cavity, thereby maintaining the temperature of the reactor itself. In the case of the semi-cavity model, the average outer wall temperature of the reactor is 993 °C and the maximum temperature is 1118 °C. However, in the full-cavity model, the average outer wall temperature is 1213 °C and the maximum temperature is 1316 °C. Therefore, the convective heat loss is reduced by approximately 2.3 kW in the full-cavity model, in comparison to the semi-cavity model.

With each model, the amount of radiation emitted from the reactor to the outside is calculated using Equations (8) and (9), and the view factor from the reactor to the outside of the cavity, based on Equation (9), is shown in Table 5. Comparing the view factors of the semi-cavity and the full cavity, it can be observed that the view factor of the full cavity has been reduced to approximately 47% of that of the semi-cavity.

Table 5. View factor (from reactor to environment).

Item	Value
semi-cavity	0.1423
full cavity	0.0670

Considering that the outer wall temperature of the reactor, in the aforementioned full cavity, increases by 220 °C, on average, and the radiation is proportional to the fourth power of the temperature, in the case of the full cavity, the radiation loss can increase by approximately 1.9-fold. However, this is nearly the same for the amount of radiation loss because the view factor from the outer wall of the reactor to the outside is reduced by approximately two-fold, from 0.1423 to 0.0670, compared to the semi-cavity. As a result, despite the change from the semi-cavity to full cavity to reduce heat loss, there is no difference in the amount of radiation loss. In other words, even if the wall temperature of the reactor is increased by more than 200 °C, the radiation loss is almost the same, and the total heat loss is reduced by 2.19 KW, even though the entire temperature environment inside the cavity is maintained at a high temperature.

Therefore, when comparing the full cavity with the semi-cavity, the difference in heat loss is 2.19 kW, and it can be observed that 9% more heat is supplied to the reactor. In addition, the more important point is that changing the cavity shape is more effective to increase the conversion rate, by maintaining a high temperature, than the advantage obtained by reducing the amount of heat loss.

4.2. Methane Conversion Rate

Based on Table 1, which shows the characteristics of the BP-2000 catalyst used in the reaction, the methane conversion rate, calculated according to residence time and catalyst temperature, is shown in Figure 18.

For the initial methane conversion, the following equation is used:

$$Initial\ methane\ conversion(\%) = [1 - \exp(-residence\ time \times k_r)] \times 100 \qquad (12)$$

To activate the catalyst, a temperature of over 700 °C is required when the residence time is 4 s, and the temperature increases as the residence time decrease. In order to obtain a conversion rate of 80% or more through methane decomposition, a reactor temperature over 1175 °C is required at a residence time of 0.1 s, as shown by the right end graph line in Figure 18. On the other hand, a relatively low reactor temperature of over 950 °C is required at a residence time of 4.0 s, as shown by the left end graph line in Figure 18. Increasing the residence time lowers the reaction temperature, which, in turn, reduces the reactor damage. However, this requires an increase in the size of the reactor, which also increases the heat transfer area for heat loss. In addition, as the reactor size can be limited by the focal size applied from the parabolic reflector, it is difficult to lower the reaction temperature by increasing the size of the reactor. Therefore, it is important to reduce heat loss by increasing the insulating performance of structures such as the cavity and reducing the opening area of the aperture, and maintaining the temperature in the reactor at a suitable temperature for the reaction.
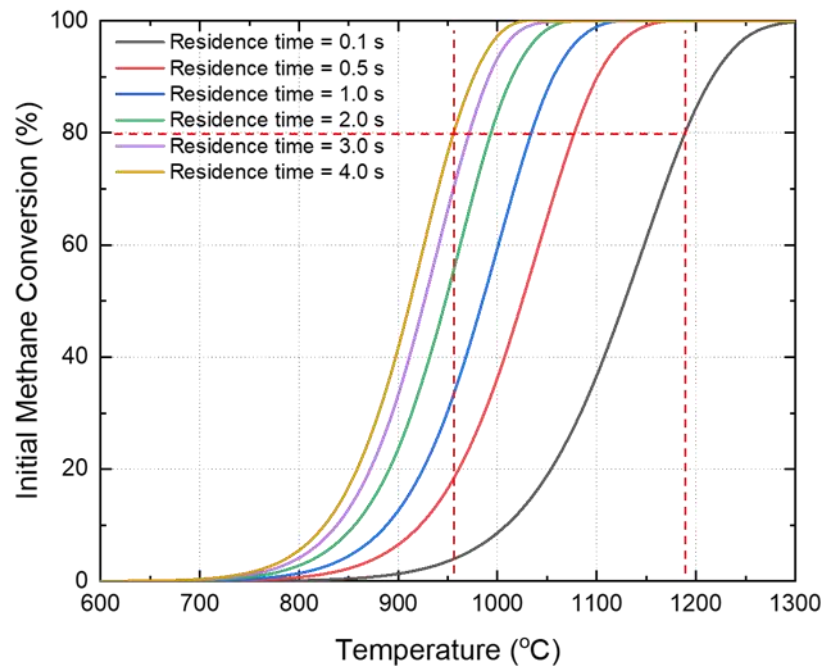
Figure 18. Effect of residence time and temperature on the initial methane conversion using BP-2000.

Figure 19 shows the distribution of the methane mass fraction in each reactor, and represents the region where the temperature is maintained above 1000 °C. The temperature and methane conversion rate, according to the catalyst height, for the semi-cavity are shown in Figures 20 and 21. The methane conversion rate is defined as one minus the methane mass fraction. In the model, the average temperature at a height of 300 mm is 678 °C, at which temperature methane is difficult to decompose, and thus the methane conversion rate is approximately 0.2%. At a height of 240 mm, the average temperature is 886 °C and the conversion rate to this height is 2.1%. In the range of 180–0 mm, the catalyst temperature rises to 1000 °C or more, but the residence time in this region is 1.1 s, which is insufficient based on Figure 18, and thus the methane conversion rate at the outlet reaches 66.5%.
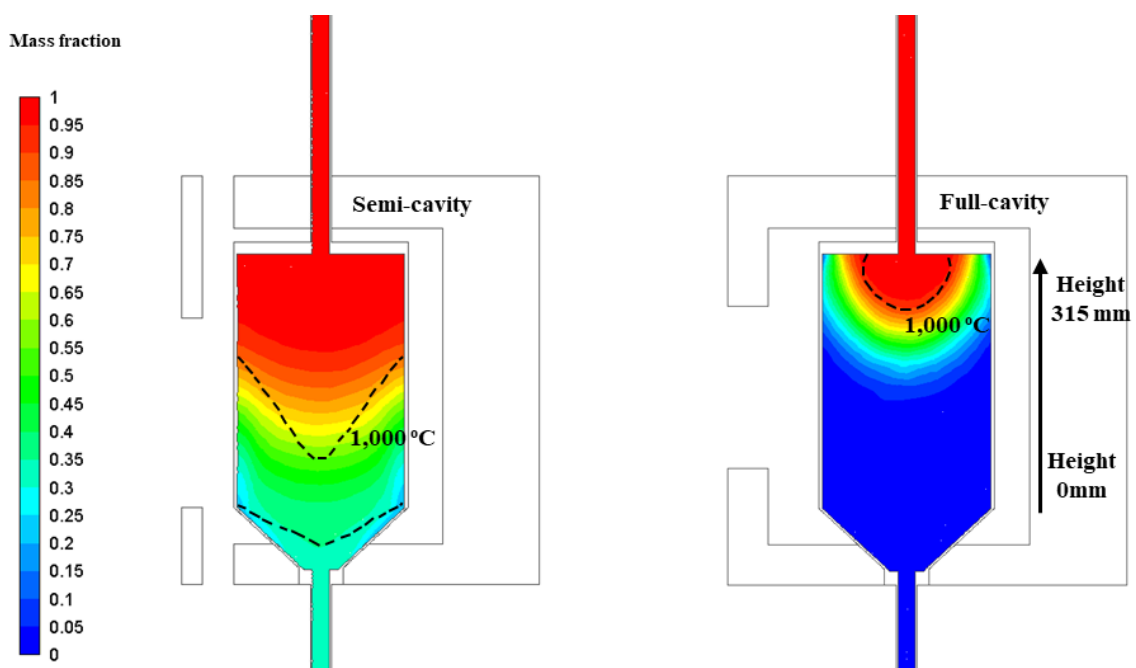

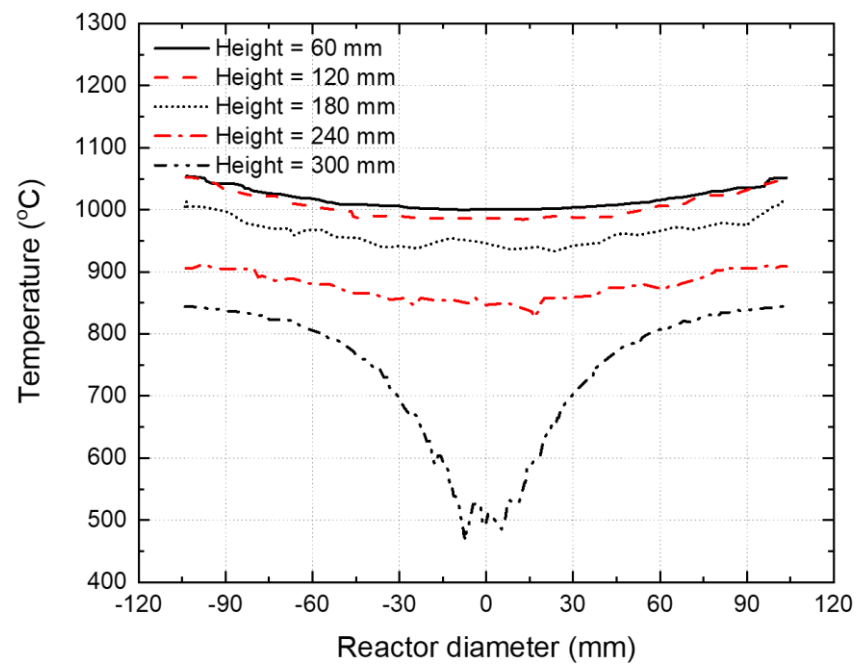**Figure 19.** Methane mass fraction contour of center vertical cross-section of two reactors.

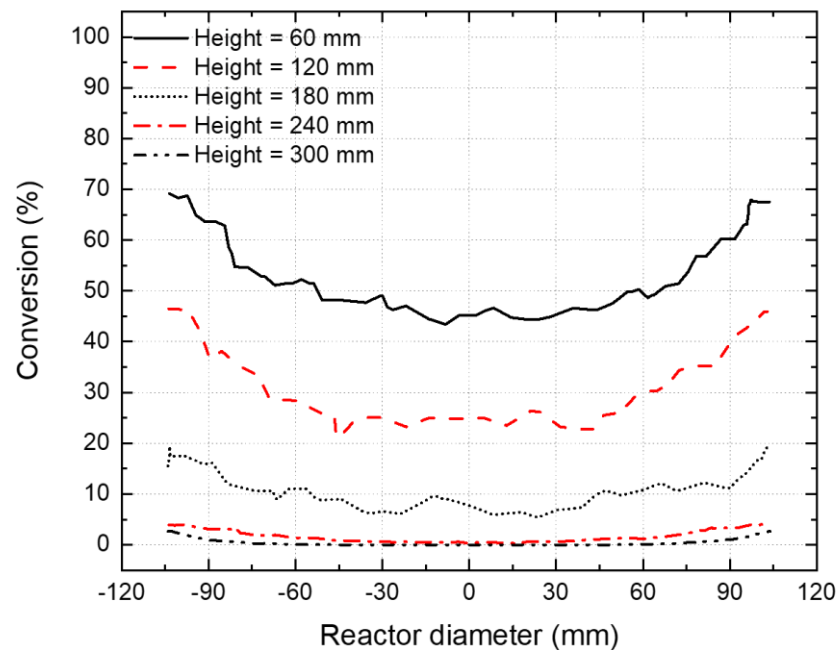**Figure 20.** Temperature distribution by height in the reactor (semi-cavity).

Figure 21. Methane conversion rate by height in the reactor (semi-cavity).

The temperature and methane conversion rate, according to the catalyst height, for the full cavity are shown in Figures 22 and 23. At a height of 300 mm near the entrance, the average temperature is 850 °C and the inner wall temperature is 1095 °C. Here, the temperature increases above 1000 °C from the outer area, with a diameter of 100 mm, to the inner wall. From this section, methane is gradually decomposed, and the conversion rate is 8.6%. At a height of 240 mm, the wall temperature is 1165 °C, the average catalyst temperature is 1087 °C, and the conversion rate reaches 51.2%. After that, the catalyst temperature in a range of height of 180–0 mm is maintained at above 1100 °C, and the residence time is 1.0 s. The residence time in this section is similar to that of the semi-cavity model; however, because the average temperature is higher than 200 °C, most of the

methane can be decomposed, as shown in Figure 18. Finally, the methane conversion at the outlet of the reactor is 99.99%.
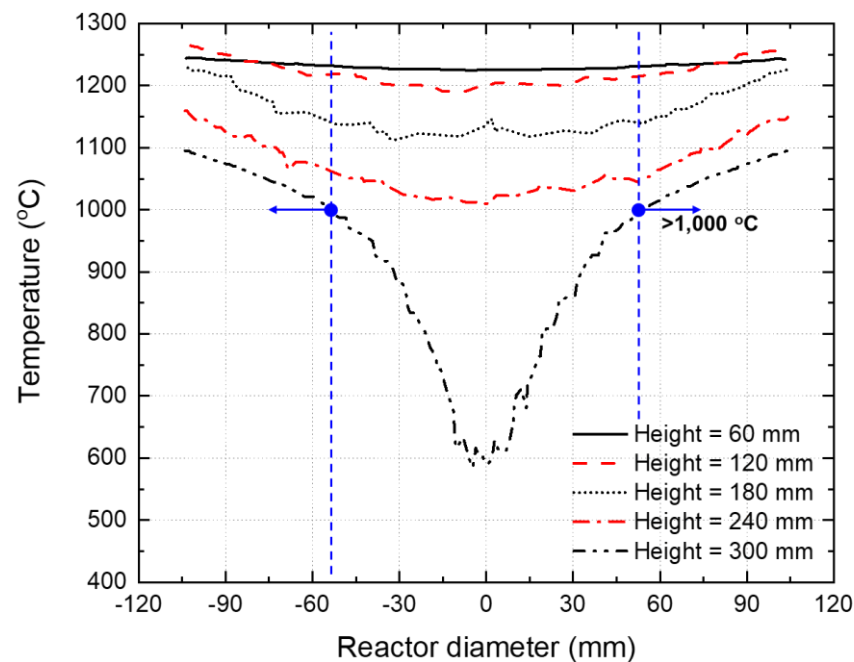

Figure 22. Temperature distribution by height in the reactor (full cavity).
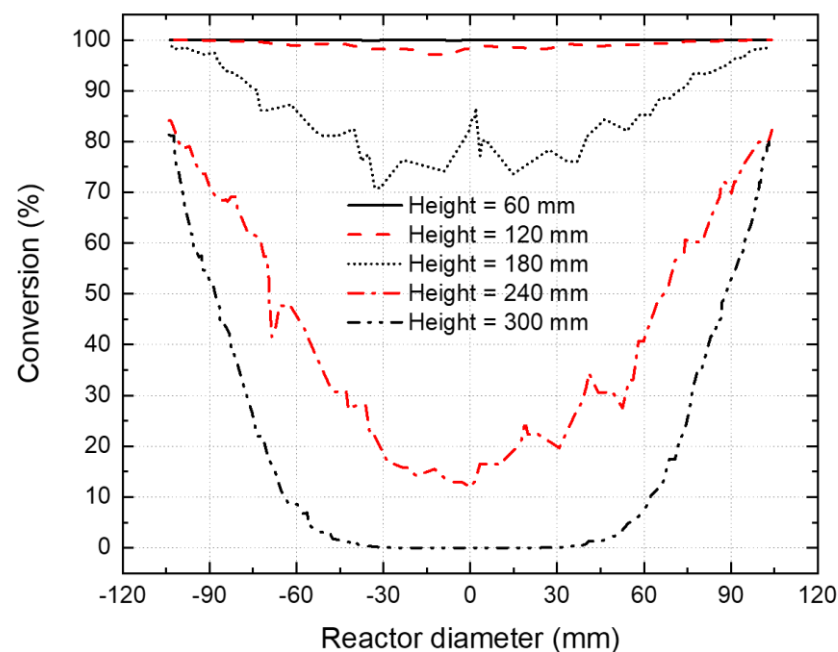

Figure 23. Methane conversion rate by height in the reactor (full cavity).

In each reactor model, the thermal amounts for the heating of methane in the reactor and the chemical reaction for thermal decomposition are shown in Table 6. In the case of a semi-cavity, a total of 7.22 kW is required for the heating and chemical reaction, and in the case of a full cavity, 9.42 kW is required. The difference is 2.2 kW, which is almost the same as the difference in the heat loss between the models, and it can be observed that the reduced heat loss at the full cavity was used for methane heating and decomposition in the reactor. As a result, the heat loss in the full cavity, compared to the semi-cavity, is reduced by 12.5%, and the conversion rate in the full cavity is increased by 33.49%.

Table 6. Thermal amount for heating and chemical reaction according to cavity model.

	Semi-Cavity	Full Cavity
Item	Thermal Amount (kW)	Thermal Amount (kW)
heating methane	4.24	5.02
Chemical reaction	2.98	4.40
total	7.22	9.42

Apparently, it can be observed that the reduction in heat loss has a significant effect on the improvement of reactor performance. However, the reason that there is a lot of improvement in the performance, in spite of the small heat loss reduction, is that the high-temperature environment could be maintained by changing the cavity shape, and it was not accompanied by an increase in heat loss.

5. Conclusions

In this study, the optical distribution, heat and transfer, and chemical reaction are numerically calculated according to the cavity model, for the development of a methane decomposition solar reactor using an indirect catalyst heating method. The cavity model is divided into a full cavity and a semi-cavity, and the heat loss and methane conversion are compared for the two models, under the same heat source and ambient conditions.

As a result, when 5 Nm^3/h of methane is supplied to the reactor, the losses owing to radiation and convection in the full cavity and semi-cavity are 15.29 and 17.48 kW, respectively, even though the wall temperature of the reactor is increased by more than 200 °C in the full cavity, the radiation loss is almost the same, the total heat loss is reduced by 2.19 kW, and the methane conversion rates are 99.99% and 66.5%, respectively. It was confirmed that the heat loss of the full-cavity model decreased by 12.5% and the methane conversion rate increased by 33.5%, compared to the semi-cavity model.

The reason that there is a lot of improvement in the performance, even with a small reduction in heat loss, is that a high-temperature environment can be maintained in the full cavity through shape change, and, despite this, there is no increase in heat loss in the full cavity. Therefore, it is expected that better results will be obtained through the optimization of openings and cavity shapes to maintain a high temperature in the reactor and reduce heat loss. In addition, as numerical research using optical calculation results for reaction calculations is possible, it can be usefully utilized when conducting experimental research through prior research on various conditions.

Nomenclature

A	Surface area, m^2
$C_{1\varepsilon}$, $C_{2\varepsilon}$, C_μ	Standard k-ε model constants
c_p	Specific heat at constant pressure, J/kg $\cdot$ K
E	Total energy, J
E_a	Activation energy, kJ/mol
F	View factor
$\vec{F}$	Force vector, N
G_b	Effect of buoyancy, J/m^3/s
G_k	Production of turbulence kinetic energy, J/m^3/s
$\vec{g}$	Gravitational acceleration, m/s^2
h	Static specific enthalpy per unit mass, J/kg
ΔH^o_{298}	Standard enthalpy of reaction, kJ/mol
$\vec{J}_i$	Diffusion flux of species I, kg/m^2 $\cdot$ s
$\vec{J}_j$	Diffusion flux of species j, kg/m^2 $\cdot$ s
k	Kinetic energy per unit mass, J/kg; thermal conductivity, W/m $\cdot$ K
k_0	Pre-exponential factor, s^{-1}
k_{eff}	Effective conductivity, W/m $\cdot$ K
k_r	Rate constant, s^{-1}
k_t	Turbulent thermal conductivity, W/m $\cdot$ K
p	Pressure, Pa
q	Heat flux, W/m^2
R	Gas law constant, J/kmol $\cdot$ K
R_i	Volumetric rate of production of species i
r	Radial distance, m
S_{rad}	Energy source of radiation
S_{reac}	Energy source of reaction
T	Temperature, K
t	Time, s
u	Velocity magnitude, m/s
$\vec{v}$	Overall velocity vector, m/s
Y_i	Mass fraction of each species
Greek Symbols	
ε	Turbulent dissipation rate, m^2/s^3; emissivity
μ	Dynamic viscosity, Pa $\cdot$ s
μ_t	Turbulent viscosity, Pa $\cdot$ s
ρ	Density, kg/m^3; Reflectivity
σ	Stefan–Boltzmann constant, W/m^2 $\cdot$ K^4
σ_k	Turbulence Prandtl number for kinetic energy
σ_ε	Turbulence Prandtl number for dissipation
$\bar{\bar{\tau}}$	Stress tensor, Pa
$\bar{\bar{\tau}}_{eff}$	Effective stress tensor, Pa

References

1. Abbas, H.F.; Wan Daud, W.M.A. Hydrogen production by methane decomposition: A review. *Int. J. Hydrog. Energy* **2010**, *35*, 1160–1190. [CrossRef]
2. Koumi Ngoh, S.; Njomo, D. An overview of hydrogen gas production from solar energy. *Renew. Sustain. Energy Rev.* **2012**, *16*, 6782–6792. [CrossRef]
3. Villafán-Vidales, H.I.; Arancibia-Bulnes, C.A.; Riveros-Rosas, D.; Romero-Paredes, H.; Estrada, C.A. An overview of the solar thermochemical processes for hydrogen and syngas production: Reactors, and facilities. *Renew. Sustain. Energy Rev.* **2017**, *75*, 894–908. [CrossRef]
4. Abanades, S.; Flamant, G. Solar hydrogen production from the thermal splitting of methane in a high temperature solar chemical reactor. *Sol. Energy* **2006**, *80*, 1321–1332. [CrossRef]
5. Abanades, S.; Flamant, G. Experimental study and modeling of a high-temperature solar chemical reactor for hydrogen production from methane cracking. *Int. J. Hydrog. Energy* **2007**, *32*, 1508–1515. [CrossRef]

6. Maag, G.; Zanganeh, G.; Steinfeld, A. Solar thermal cracking of methane in a particle-flow reactor for the co-production of hydrogen and carbon. *Int. J. Hydrog. Energy* **2009**, *34*, 7676–7685. [CrossRef]

7. Hirsch, D.; Steinfeld, A. Solar hydrogen production by thermal decomposition of natural gas using a vortex-flow reactor. *Int. J. Hydrog. Energy* **2004**, *29*, 47–55. [CrossRef]

8. Ozalp, N.; Jayakrishna, D. CFD analysis on the influence of helical carving in a vortex flow solar reactor. *Renew. Energy* **2010**, *35*, 6248–6260. [CrossRef]

9. Yeheskel, J.; Epstein, M. Thermolysis of methane in a solar reactor for mass-production of hydrogen and carbon nano-materials. *Carbon* **2011**, *49*, 4695–4703. [CrossRef]

10. Rodat, S.; Abanades, S.; Coulié, J.; Flamant, G. Kinetic modelling of methane decomposition in a tubular solar reactor. *Chem. Eng. J.* **2009**, *146*, 120–127. [CrossRef]

11. Rodat, S.; Abanades, S.; Sans, J.L.; Flamant, G. Hydrogen production from solar thermal dissociation of natural gas: Development of a 10 kW solar chemical reactor prototype. *Sol. Energy* **2009**, *83*, 1599–1610. [CrossRef]

12. Rodat, S.; Abanades, S.; Sans, J.L.; Flamant, G. A pilot-scale solar reactor for the production of hydrogen and carbon black from methane splitting. *Int. J. Hydrog. Energy* **2010**, *35*, 7748–7758. [CrossRef]

13. Valdés-Parada, F.J.; Romero-Paredes, H.; Espinosa-Paredes, G. Numerical simulation of a tubular solar reactor for methane cracking. *Int. J. Hydrog. Energy* **2011**, *36*, 3354–3363. [CrossRef]

14. Muradov, N. Thermocatalytic CO2-Free Production of Hydrogen from Hydrocarbon Fuels. In Proceedings of the 2000 Hydrogen Program Review, NREL/CP- 570-28890, San Ramon, CA, USA, 9–11 May 2000.

15. Muradov, N.; Smith, F.; T-Raissi, A. Catalytic activity of carbons for methane decomposition reaction. In Proceedings of the Catalysis Today; Elsevier: Amsterdam, The Netherlands, 2005; Volume 102–103, pp. 225–233.

16. Suelves, I.; Pinilla, J.L.; Lázaro, M.J.; Moliner, R. Carbonaceous materials as catalysts for decomposition of methane. *Chem. Eng. J.* **2008**, *140*, 432–438. [CrossRef]

17. Ashik, U.P.M.; Wan Daud, W.M.A.; Hayashi, J.I. A review on methane transformation to hydrogen and nanocarbon: Relevance of catalyst characteristics and experimental parameters on yield. *Renew. Sustain. Energy Rev.* **2017**, *76*, 743–767. [CrossRef]

18. Abanades, S.; Kimura, H.; Otsuka, H. Kinetic investigation of carbon-catalyzed methane decomposition in a thermogravimetric solar reactor. *Int. J. Hydrog. Energy* **2015**, *40*, 10744–10755. [CrossRef]

19. Lee, H.; Chai, K.; Kim, J.; Lee, S.; Yoon, H.; Yu, C.; Kang, Y. Optical performance evaluation of a solar furnace by measuring the highly concentrated solar flux. *Energy* **2014**, *66*, 63–69. [CrossRef]

20. Wallen, C.W. *Astrophysical Quantities*, 3rd ed.; Athlone Press: London, UK, 1973; pp. 169–171.

21. Buie, D.; Monger, A.G.; Dey, C.J. Sunshape distributions for terrestrial solar simulations. *Sol. Energy* **2003**, *74*, 113–122. [CrossRef]